WATERTOWN ARSENAL
LABORATORY

Division of Engineering
BROWN UNIVERSITY
PROVIDENCE, R. I.

AD A951007
DTIC FILE COPY

THE LOAD CARRYING CAPACITY OF CIRCULAR PLATES AT LARGE DEFLECTION

BY

E. T. ONAT AND R. M. HAYTHORNTHWAITE

AD-A050920
DTIC
ELECTE
SEP 14 1981
S D
A

This document has been approved for public release and sale; its distribution is unlimited.

U.S. Army Ordnance Corps
Office of Ordnance Research
Contract DA-19-020-ORD-3172
Project TB 2 0001(1036)
Tech. Rept. 4 December, 1954

WAL, ARO
ORD-3172/4
81 9 10 095

NOTE:-This form is to be executed to show proposed distribution, and forwarded in triplicate to the Chief of Ordnance for prior approval of all distributions. Proposed distribution to agencies or individuals whose official interest in the report is not obvious must be justified by explanatory statements on the back of this form.

BINDING AREA FORM NO. ORDBE-342L. (Rev.) 2 Sept. 1947 *BINDING AREA*

COPIES PREPARED 4

EXTRA COPIES REMAINING

WATERTOWN ARSENAL

TECHNICAL REPORT DISTRIBUTION

REPORT NO. 140/19-6 TITLE: Brown University DA...3172 DA...3172 Tech. Rpt. No. 4.

TO:	NO. OF COPIES	DATE OCO APPROVAL	DATE SENT	TO:	NO. OF COPIES	DATE OCO APPROVAL	DATE SENT
WATERTOWN ARSENAL-ORDBE				OTHER:			
Laboratory File	1						
~~Author:~~ J. Bluhm	1	#2					
OFFICE, CHIEF OF ORDNANCE							
ORDIR-Artillery							
ORDIM-Ammunition							
ORDIT-Automotive							
ORDIS-Small Arms							
ORDTB-Res. & Materials							
ORDTM-Ammunition Dev.							
ORDTR-Artillery Dev.							
ORDTS-Small Arms Dev.							
ORDTT-Tank Automotive							
ORDTU-Rocket Dev.							
ORDTX-Executive							
ORDTX-AR - Executive Library	1						
ORDNANCE DEPARTMENT AGENCIES							
ORDBA-Frankford Arsenal							
ORDBB-Picatinny Arsenal							
ORDBC-Rock Island Arsenal							
ORDBD-Springfield Armory							
ORDBF-Watervliet Arsenal							
ORDBG-Aberdeen Prov. Ground							
ORDJR-Raritan Arsenal							
ORDMX-Detroit Arsenal							

APPROVING AUTHORITY:

Ltr.:

Date:

From:

The Load Carrying Capacity of Circular Plates at Large Deflection[1]

by

E. T. Onat[2] and R. M Haythornthwaite[3]

Abstract

This paper presents an approximate analysis for the load carrying capacities of initially flat circular plates under various loading and edge conditions and subjected to slowly increasing load. As a plate deforms the carrying capacity is increased due to favourable changes in geometry. The load capacity is estimated by assuming a velocity field based on the boundary conditions and on the incipient velocity field of the flat plate. The analysis is made for a rigid plastic, non strain-hardening material that yields according to the maximum shear stress criterion. In several cases the results obtained compare favourably with published test data for mild steel plates; however, for very thin plates, better agreement is obtained by means of a purely membrane type analysis, which is also presented.

---

1. The results presented in this paper were obtained in the course of research sponsored by the Office of Ordnance Research under Contract No. DA-19-020-ORD-3172, Project No. TB2-0001 (1086).

2. Research Associate, Division of Applied Mathematics, Brown University, Providence, R. I.

3. Assistant Professor, Division of Engineering, Brown University, Providence, R. I.

Contract DA-19-020-ORD-3172/4
Project No. TB2-0001 (1086)

Codes
Dist | Avail and/or Special
A
UNANNOUNCED

Introduction

The analysis presented in this paper was prompted by the results of recent static loading tests on circular mild steel plates in the plastic range [1,2,3,4][4]. In each of these tests, the rate of increase of deflection did not approach the indefinitely high value expected from the usual theory of limit analysis [5]. Instead, the load continued to increase without excessive deflection to well above the expected collapse load. The explanation of this will be sought through a study of the load-deflection relationship in the plastic range. The approach adopted may in itself prove useful as the basis of a more comprehensive technique for the limit analysis of plates.

The methods of limit analysis [5,6] enable good estimates to be made of the useful carrying capacity of certain structural steel frameworks in which instability does not develop and in which unserviceability due to excessive deflection occurs before any member fails due to fracture. Tests have shown these to include, for example, some single span and multi-span beams [7,8,9] and some portal frames [10] fabricated from low carbon structural steel. In the theory, elasticity of the material is usually neglected and the load carrying capacity is estimated as the load at which a model composed of an ideal, rigid-plastic material would begin to deform. It can be shown that, if the material is perfectly plastic (i.e. non-strain hardening) and if the accompanying change in geometry is disregarded, plastic flow continues under constant load [6]. Thus, under monotonically increasing load, the rigid-plastic model collapses as soon as the yield point load is reached, and this reflects quite accurately the observed behaviour of structures of the types referred to.

The simplest limit analysis theory neglects both strain hardening and changes in geometry and this must always be borne in mind when attempting

---

4. Numbers in square brackets refer to the bibliography at the end of the paper.

Contract DA-19-020-ORD-3172/4
Project TB2-0001 (1086)

to broaden its field of application. When either of these factors is introduced in the theoretical model, it is found that, in general, plastic flow can continue only under either increasing or decreasing load [11]. If the modified model is appropriate, the yield load may then be of less value as a measure of the carrying capacity of the actual structure. In practice, the rate of increase of deflection with load will usually be the significant factor. When this rate greatly exceeds the rate of deflection in the elastic range the structure will rapidly become unserviceable and the practical limit of carrying capacity will have been reached. This stage can be identified by investigating the load-deflection relationship beyond the yield load.

The above considerations lead us to suppose that the observed post-yield behaviour of circular plates is probably conditioned by change of geometry and by strain hardening. In this paper the role of the change of geometry will be investigated and the resulting theoretical load deflection curves will be compared with the results of tests. The distorted plate is an example of a rotationally symmetric shell and the mathematical problem of determining the limit load of such a shell will be reviewed as a basis for the further discussion. Only rotationally symmetric, monotonically increasing loading will be considered. The case of reversing loads is discussed elsewhere [12].

2. Quasi-Static Deformations of an Initially Flat Rigid-Plastic Plate as a Problem of Plastic Shell Theory.

Consider a circular plate made of rigid plastic material and subjected to a rotationally symmetrical, monotonically increasing load that can be described by a single parameter. As the intensity of this loading is raised gradually, starting from zero, the plate at first remains rigid. It begins to deform when the load reaches a critical value, termed the limit load [5] or

the yield load [11]. Let us assume that the loads are varied in such a manner that the further distortion following the reaching of the yield load takes place in a quasi-static manner. Because of the symmetry of the loading and edge conditions, the plate will assume a shape that is axially symmetrical with respect to the axis of symmetry of the original shape. Thus the initially flat plate becomes a shell of revolution for the post yield point loads. Now, if it is assumed that the material is ideally plastic, then at each instant we have to consider an equilibrium state for a quasi-static shell of revolution.

Fig. (1) shows an element of such a shell with the stress resultants transmitted across the boundary meridians and parallels; M_φ and M_θ are the meridional and circumferential bending moments, N_φ and N_θ the corresponding membrane forces, and Q the shear force, each measured per unit length of shell cross-section. The load per unit area of the middle surface of the shell has the components λY in the direction of the meridian and λZ in the direction of the normal. Y and Z are supposed to be known and λ is the unknown load parameter. The arrows in Fig. (1) indicate the conventions for positive forces and couples. The equilibrium of the shell element requires that

$$\left.\begin{aligned} &(r_0 N_\varphi)' - r_1 N_\theta \cos\varphi - r_0 Q + r_0 r_1 \lambda Y = 0 \\ &(r_0 N_\varphi) + r_1 N_\theta \sin\varphi + (r_0 Q)' + r_0 r_1 \lambda Z = 0 \\ &(r_0 M_\varphi)' - r_1 M_\theta \cos\varphi - r_0 r_1 Q = 0. \end{aligned}\right\} \qquad (1)$$

where the prime denotes differentiation with respect to φ.

To obtain the velocity field of the plastic flow, the particles originally on the normal to the undeformed middle surface are assumed to remain on a normal to the middle surface as the latter is deforming. When the motion of the middle surface is known, the velocity field of the plastic flow and also the plastic strains are then determined.

Contract DA-19-020-ORD-3172/4
Project TB2-0001 (1086)

Consider a generic point A, Fig. (2), situated at a distance ξ from the centre of the plate before the plastic deformations set in. This point will have the co-ordinates $r(\xi, t)$ and $z(\xi, t)$ at time t and

$$r(\xi, 0) = \xi \qquad \text{and} \qquad z(\xi, 0) = 0 .$$

If the meridional and normal velocities are denoted by v and w respectively, the positive directions being those indicated by Y and Z in Fig. (1), these components can be expressed in terms of $\dot{r}$, $\dot{z}$, r and z where the dot denotes time differentiation. The principal rates of strain in the middle surface are

$$\varepsilon_\varphi = \frac{1}{r_1}(v' - w); \qquad \varepsilon_\theta = \frac{1}{r_2}(v \cot\varphi - w) . \tag{2}$$

The principal rates of curvature are

$$\varkappa_\varphi = + \frac{1}{r_1}\left[\frac{1}{r_1}(v + w')\right]'; \qquad \varkappa_\theta = + \frac{\cot\varphi}{r_1 r_2}(v + w') \tag{3}$$

where the prime denotes differentiation with respect to φ.

The plastic behaviour of the shell is described completely by the field quantities M_φ, M_θ, N_φ, N_θ and $r(\xi, t)$ and $z(\xi, t)$. They are functions of position and time. Note that any monotonically increasing function, such as the deflection of the centre of the plate or the load intensity λ, can be used as the measure of time.

Plastic deformation may take place wherever the state of stress is represented by a point on the yield hypersurface

$$f\left(\frac{N_\varphi}{N_0}, \frac{N_\theta}{N_0}, \frac{M_\varphi}{M_0}, \frac{M_\theta}{M_0}\right) = 0 \tag{4}$$

where $M_0 = \frac{1}{4}\sigma_0 h^2$, & $N_0 = \sigma_0 h$, σ_0 being the yield stress of the material in simple tension and h the thickness of the plate. The hypersurface $f = 0$

Contract DA-19-020-ORD-3172/4
Project TB2-0001 (1086)

has been described in detail for a material obeying the maximum shear stress yield criterion [13]. The condition that work is absorbed in the plastically deforming parts demands that (4) is always convex and that the flow mechanism and the state of stress (represented by the generalized stresses N_φ/N_0 etc.) are related by the flow rule

$$N_0\varepsilon_\varphi : N_0\varepsilon_\theta : M_0\varkappa_\varphi : M_0\varkappa_\theta = \frac{\partial f}{\partial\left(\frac{N_\varphi}{N_0}\right)} : \frac{\partial f}{\partial\left(\frac{N_\theta}{N_0}\right)} : \frac{\partial f}{\partial\left(\frac{M_\varphi}{M_0}\right)} : \frac{\partial f}{\partial\left(\frac{M_\theta}{M_0}\right)} . \tag{5}$$

Geometrically, (5) states that, at a generic point of the yield hypersurface $f = 0$, the vector with components proportional to $N_0\varepsilon_\varphi$, $N_0\varepsilon_\theta$, $M_0\varkappa_\varphi$ and $M_0\varkappa_\theta$ (drawn in the directions N_φ/N_0, N_θ/N_0, M_φ/M_0 and M_θ/M_0 respectively) will have the same direction as the exterior normal to the yield hypersurface at the point considered. For any parts of the shell that are at rest or undergo rigid body motion the corresponding stress points will be within the yield hypersurface.

We now recapitulate the equations and conditions to be satisfied by the field quantities: it is required to find functions N_φ, N_θ, M_φ, M_θ, Q, $r(\xi,t)$ and $z(\xi,t)$ in such a way that

1) $N_\varphi(\varphi,t)$, $N_\theta(\varphi,t)$, $M_\varphi(\varphi,t)$, $M_\theta(\varphi,t)$ and $Q(\varphi,t)$ satisfy the equations of equilibrium (1) the coefficients of which are functions of $r(\xi,t)$ and $z(\xi,t)$.

2) All points with co-ordinates $\frac{N_\varphi}{N_0}$, $\frac{N_\theta}{N_0}$, $\frac{M_\varphi}{M_0}$, and $\frac{M_\theta}{M_0}$ lie inside or on the yield surface (4). In the first case the shell must remain at rest or perform rigid body motion; in the second case the strain rates defined by the equations (2) and (3) must satisfy the flow rule

(5).

3) The boundary conditions and some additional regularity conditions must be satisfied.

3. A Basis for Approximate Solutions

The mathematical problem described in the previous section is rather complicated. The yield condition (4) may be a non-linear algebraic equation; hence also the flow rule (5) may be non-linear. The equilibrium equations (1) contain coefficients that are functions of the unknown coordinates $r(\xi,t)$ and $z(\xi,t)$.

In the case of the undeformed plate the latter difficulty does not arise. Also, if Tresca's yield condition is used, the equations of equilibrium may be integrated directly and the complete solution obtained, including the incipient velocity field and the stress distribution at the yield point [14]. For example, a simply supported circular plate carrying a load concentrated at the centre will begin to deform plastically when the load reaches the yield or limit load $2\pi M_0$*. The velocity field that initiates the plastic distortion is given by

$$\left.\begin{aligned} w &= c\left(1 - \frac{\xi}{R}\right) \\ v &= 0 \end{aligned}\right\} \tag{6}$$

where c is an undetermined positive constant and R is the radius of the plate.

If now the early stages of the plastic deformation are considered the velocity field may be expected to differ only slightly from the field given by (6); hence the shape of the middle surface after a time interval t may be approximated by

*The effect of shear is neglected.

Contract DA-19-020-ORD-3172/4
Project TB2-0001 (1086)

$$z = ct\left(1 - \frac{\xi}{R}\right) \tag{7}$$

where ct may be chosen as small as desired. The equation (7) then suggests that the initially flat plate will become a conical shell.

Actual tests of mild steel plates loaded through a central punch have shown that the deformed shape remains very nearly conical even when the permanent deflection is several times the thickness [3,4]. Other tests using various loading and edge conditions have shown that in each case the deformed shape can be approximated by continuing the incipient velocity field obtained at zero deflection [3].

The facts mentioned above point to a method of attack that may be used to obtain approximate solutions. If a velocity field can be found that describes the position of the midsurface of the plate at every stage with reasonable accuracy, then the applied loads associated with it might be used as estimates of the carrying capacity of the plate. Before this can be done, reasonable assumptions must be made concerning the radial component of the velocity. Here the force or velocity boundary conditions at the support are a valuable guide.

Once both components of the velocity field have been chosen, the rates of strain e_θ, e_φ for every point in the plate follow from (2) and (3) by

$$e_\theta = \varepsilon_\theta + \varkappa_\theta z; \qquad e_\varphi = \varepsilon_\varphi + \varkappa_\varphi z.$$

The rate of dissipation of energy can be computed and the magnitude of the applied load follows at once by virtual work. In this approach, no use is made of the equilibrium equations, so the forces N_φ, N_θ, M_φ and M_θ need not be computed. Instead the rate of energy dissipation is found directly

from the strain rates and the corresponding stresses.

The components Y and Z of the exterior load are given to within a common factor λ that defines the unknown critical load intensity. Since no energy is recoverable from a rigid-plastic shell, the total rate of energy dissipation must equal the rate at which the applied unit loads (multiplied by λ) do work. This condition is satisfied if λ is determined from

$$\lambda \left| \int (vY + wZ)\, r_0 r_1 d\varphi \right| = \int D\, r_0 r_1 d\varphi \qquad (8)$$

where D is the rate of dissipation of energy per unit area and the integration is extended over the entire meridian. In the following, equation (8) will be used to give an estimate of the load intensity λ. Once the approximate mode of deformation is decided upon with the help of the incipient velocity field and the boundary conditions, then r_0 and r_1 and hence v and w may be computed as functions of φ and a time-like parameter, such as the maximum deflection δ. Equation (8) gives the load intensity parameter λ in terms of δ, thus establishing a load-deflection relationship for the post yield-point loads.

This approach will now be applied to two cases for which test data is available. For the purpose of analysis, the ideal material is assumed to yield according to the maximum shear stress criterion and subsequently to obey the corresponding flow rule. The rate of energy dissipation per unit volume during plastic flow is $\sigma_0 |e|_{max.}$ where σ_0 is the yield stress in simple tension and $|e|_{max.}$ is the greatest principal strain rate. The use of the maximum shear stress criterion results in particularly straight-forward algebra; but any other criterion could be employed without introducing any basic difficulty. The corresponding incipient velocity field would have to be known, of course.

Contract DA-19-020-ORD-3172/4
Project TB2-0001 (1086)

Example I. The Simply Supported Circular Plate.

Consider a circular plate of uniform thickness h, simply supported at the outer radius $r = R$ and carrying a lateral load of intensity p applied to a central circular zone of radius $r = a$, as shown in Fig. (2). As mentioned already, the incipient velocity distribution at the limit load will tend to deform the plate into a right circular cone with apex at the center. This is known to be correct only at zero deflection, when there are no membrane forces. The conical shape might reasonably be taken as a first approximation during small but finite deflections. The membrane forces are no longer zero and must be considered when computing the loads required to produce the deformation; also these forces satisfy boundary conditions with which any assumed velocity field should be made to fit, as far as is possible.

The assumption of a conical shape for the deformed plate serves to fix one component of the velocity distribution— that normal to the plate at any instant. The component in the plane of the plate has yet to be fixed. If the plate is freely supported at the outer edge, radial membrane force at the edge will be zero; hence the corresponding velocity component is probably small. Thus a reasonable assumption would seem to be to set the velocity component in the plane of the plate zero at the outer edge. For simplicity, the component will be taken as zero throughout the plate, but the more general case could be treated on similar lines. The material point initially at A_0, Fig. (2), will move to A. The circumferential strain on the mid-surface is $\cos\varphi - 1 \approx -\varphi^2/2$ when φ is small; hence the circumferential strain rate (with respect to φ) is

$$\varepsilon_\theta \approx -\varphi \approx -\frac{\delta}{R}$$

Also $x/r_2 = \tan\varphi \approx \varphi$; so $1/r_2 \approx \varphi/x$ and the circumferential curvature rate (with respect to φ) is

$$\varkappa_\theta \approx \frac{1}{x} = \frac{1}{r}.$$

Contract DA-19-020-ORD-3172/4
Project TB2-0001 (1086)

The rate of energy dissipation per unit volume is $\sigma_0 |e|_{max.}$ where $|e|_{max.}$ is the numerically largest principal strain rate; hence the rate of energy dissipation per unit area of the plate is

$$d = \sigma_0 \int_{-h/2}^{h/2} |e|_{max} \, dz. \tag{9}$$

The only strain is in the circumferential direction so $|e|_{max} = |\varepsilon_\theta + \varkappa_\theta z|$ and by integration the area of the $|e|_{max}$ diagram, Fig. (3) is found to be

$$\frac{d}{\sigma_0} = \begin{cases} |\varkappa_\theta| \dfrac{h^2}{2} + \dfrac{\varepsilon_\theta^2}{|\varkappa_\theta|} = \dfrac{h^2}{4r} + \dfrac{\delta^2 r}{R^2} & \text{when } r \leq \dfrac{Rh}{2\delta} \quad \text{(a)} \\[2ex] |\varepsilon_\theta| h = \dfrac{\delta h}{R} & \text{when } r \geq \dfrac{Rh}{2\delta} \quad \text{(b)} \end{cases} \tag{10}$$

For small deflections $\left(\frac{\delta}{h} < \frac{1}{2}\right)$, (10a) applies throughout the plate. The total rate of energy dissipation is then

$$D = \int_0^R (2\pi r d) \, dr = 2\pi M_0 R\left(1 + \frac{4}{3}\frac{\delta^2}{h^2}\right)$$

where $M_0 = \frac{1}{4}\sigma_0 h^2$.

The rate of work by the applied pressure p is

$$E = 2\pi p \int_0^a r(R-r) \, dr = PR\left(1 - \frac{2}{3}\frac{a}{R}\right)$$

where $P = \pi a^2 p$ is the total load.

By the upper bound theorem of limit analysis [6], $E \leq D$. Writing $P_L = 2\pi M_0/(1 - 2a/3R)$ for the yield load of the undeformed plate $(\delta = 0)$,

$$\frac{P}{P_L} = \begin{cases} 1 + \dfrac{4}{3}\dfrac{\delta^2}{h^2} & \text{when } \delta/h \leq 1/2 \\[2ex] 2\dfrac{\delta}{h} + \dfrac{1}{6}\dfrac{h}{\delta} & \text{when } \delta/h \geq 1/2 \end{cases} \tag{11}$$

Contract DA-19-020-ORD-3172/4
Project TB2-0001 (1086)

Comparison with Tests.

In Fig. (6) a load-deflection curve computed by means of (11) is compared with observations of the central deflection of a simply supported mild steel plate loaded through a centrally placed punch [4]. In addition, a load-deflection curve is shown based on an approximate theory neglecting membrane stresses but allowing for the elasticity of the material [1]. A third curve has been obtained by adding to the deflection found by means of (11) an elastic deflection component proportional to the initial deflection rate.

The last mentioned curve serves to show that the slope of the experimental points at high loads is very nearly the sum of the initial elastic slope and that obtained from the use of equations (11). It must be emphasized that this superposition has been made to illustrate the good agreement with the tests thus made possible. Lateral displacement of the curve based on a rigid-plastic model has no known theoretical justification; however, when sufficient confirmatory tests are available, it might prove useful in engineering practice as a method for obtaining conservative estimates of plate deflection.

In the early stages of plasticity the approximate elastic-plastic theory is probably more satisfactory for practical applications because it will overestimate deflection, providing shear is unimportant. Nevertheless the present theory gives a much better picture of the mechanics of post yield behaviour.

Example II. The Clamped Circular Plate.

Consider a plate similar to that of example 1, but clamped to a stiff ring at its outer radius $r = R$, as shown in Fig. (7). This ring is supposed to prevent all radial and rotational movements of the outer edge.

In this case it would be unreasonable to set the rate of strain zero in the direction of the plate mid-surface. If the edges are prevented from moving inwards there must be some such strain if the plate is to deflect at all.

The simplest assumption is to set the radial velocity zero, so that all material points in the plate move vertically. A continuation of the incipient velocity field then furnishes a complete description of the movement.

The incipient velocity field is made up of two parts [14]. In a central zone bounded by $r = \rho$ the plate deforms to a conical shape, as for the simply supported plate of example 1. Outside this zone the shape is logarithmic. Finite rotation occurs just inside the clamped edge, implying the formation of a kink or plastic hinge at that radius. Defining a function $C(\delta)$ of the central deflection δ by

$$C(\delta) = \frac{\delta}{1+\ln\frac{R}{\rho}}, \tag{13}$$

the rate of deflection with respect to C is [14],

$$\dot{z} = \begin{cases} 1 + \ln\frac{R}{\rho} - \frac{r}{\rho} & \text{when} \quad 0 \leq r \leq \rho \\ \ln\frac{R}{r} & \text{when} \quad \rho \leq r \leq R. \end{cases} \tag{14}$$

When $a/R \leq e^{-1/2} = 0.606$, ρ is found from the transcendental equation

$$1 - \frac{2}{3}\frac{a}{\rho}\left(1 + \ln\frac{R}{\rho}\right) = 0 \tag{15}$$

and when $a/R \geq 0.606$, it is found from

$$1 - \frac{a^2}{\rho^2}\left(1 + 2\ln\frac{R}{a}\right) + \frac{2}{3}\left(1 + \ln\frac{R}{\rho}\right) = 0 \tag{16}$$

We shall assume that the expressions (14), known to be correct for zero deflection are a reasonable approximation when the deflection is non-zero.

Exact determination of the rates of extension and curvature of the middle surface at finite deformations is rather involved in this case. The mathematical work is simplified considerably by making the following

approximations, familiar from the elastic theory for shells,

$$-1/r_1 \approx d^2z/dr^2; \qquad \varphi \approx -dz/dr; \qquad r_2 \approx -r/(dz/dr).$$

We then obtain from (2) and (3), for $0 \leq r \leq \rho$,

$$\varepsilon_\varphi = dv/dr = +C/\rho^2$$
$$\varepsilon_\theta = \frac{1}{r_2}(v \cot\varphi - w) = 0$$
$$\varkappa_\varphi = d^2w/dr^2 = 0$$
$$\varkappa_\theta = (dw/dr)/r_2 \sin\varphi = 1/\rho r$$

and for $r \leq \rho \leq R$,

$$\varepsilon_\varphi = (dv/dr)\, r_2 \cos\varphi/r_1 - w/r_1 = C/r^2$$
$$\varepsilon_\theta = 0$$
$$\varkappa_\varphi = [d(v/r_1)/dr + d^2w/dr^2]\, r_2 \cos\varphi/r_1 = -1/r^2$$
$$\varkappa_\theta = +1/r^2$$

where the rates of strain and curvature are taken with respect to C.

Fig. (4) shows the strain rate diagrams for the above. By integration of the $|e|_{max}$ diagram we obtain, for $0 \leq r \leq \rho$, Fig. (4a),

$$\frac{d}{\sigma_0} = \begin{cases} \dfrac{Ch}{2\rho^2} + \dfrac{C^2 r}{2\rho^3} + \dfrac{h^2}{4\rho r} & \text{when } \dfrac{C}{\rho} \leq \dfrac{h}{2r} \\[2ex] \dfrac{Ch}{\rho^2} + \dfrac{h^2}{8\rho r} & \text{when } \dfrac{C}{\rho} \geq \dfrac{h}{2r} \end{cases}$$

and for $\rho \leq r \leq R$, Fig. (4b),

$$\frac{d}{\sigma_0} = \begin{cases} \dfrac{Ch}{2r^2} + \dfrac{C^2}{2r^2} + \dfrac{h^2}{4r^2} & \text{when } C \leq \dfrac{h}{2} \\[2ex] \dfrac{Ch}{r^2} + \dfrac{h^2}{8r^2} & \text{when } C \geq \dfrac{h}{2}. \end{cases}$$

Contract DA-19-020-ORD-3172/4
Project TB2-0001 (1086)

The rates of energy dissipation in the parts of the plate defined by $0 \leq r \leq \rho$ and $\rho \leq r < R$ (excluding $r = R$), are then obtained by integration. Towards the edge, $dz/dr = C/R$ just inside the plate and zero at the edge itself. The resulting plastic hinge (see, for instance, [5]) requires the development of the fully plastic moment M_0 (if the effects of shear forces are neglected). The rate of energy dissipation at the plastic hinge is $2\pi R M_0 (1/R) = 2\pi M_0$. The total rate of energy dissipation is then

$$D = 2\pi M_0 + \int_0^R (2\pi r d)\, dr = 2\pi M_0 A$$

where

$$A = \begin{cases} 2 + \ln\frac{R}{\rho} + \frac{C}{h}\left(1 + 2\ln\frac{R}{\rho}\right) + \frac{C^2}{h^2}\left(\frac{2}{3} + 2\ln\frac{R}{\rho}\right) & \text{when } C \leq h/2 \\ \frac{3}{2} + \frac{1}{2}\ln\frac{R}{\rho} + \frac{C}{h}\left(2 + 4\ln\frac{R}{\rho}\right) + \frac{h}{12C} & \text{when } C \geq h/2 \end{cases} \tag{17}$$

The rate at which work is done by the pressure loading p is

$$E = \int_0^a 2\pi r \dot{z} p\, dr = BP$$

where $P = \pi a^2 p$ is the total load and

$$B = \begin{cases} 1 + \ln\frac{R}{\rho} - \frac{2a}{3\rho} & \text{when } \rho \geq a \\ \frac{1}{2} + \ln\frac{R}{a} - \frac{\rho^2}{6a^2} & \text{when } \rho \leq a \end{cases} \tag{18}$$

Employing again the upper bound theorem of limit analysis [6], $E \leq D$; hence

$$P \leq 2\pi M_0 A/B$$

where A and B are given by (17) and (18) above. The yield load of the undeformed plate is $P_L = 2\pi M_0 A_0/B$ where $A_0 = 2 + \ln\frac{R}{\rho}$; hence, on substitution

for C (equation 13) in (17),

$$\frac{P}{P_L} \leq \frac{A}{A_0} = \begin{cases} 1 + \alpha_1\left(\frac{\delta}{h}\right) + \alpha_2\left(\frac{\delta}{h}\right)^2 & \text{when } \frac{\delta}{h} \leq \frac{1}{2} + \frac{1}{2}\ln\frac{R}{\rho} \\ \beta_1 + \beta_2\left(\frac{\delta}{h}\right) + \beta_3\left(\frac{h}{\delta}\right) & \text{when } \frac{\delta}{h} \geq \frac{1}{2} + \frac{1}{2}\ln\frac{R}{\rho} \end{cases}$$

where $\alpha_1 = \dfrac{(1 + 2\ln\frac{R}{\rho})}{(2 + \ln\frac{R}{\rho})(1 + \ln\frac{R}{\rho})}$; $\alpha_2 = \dfrac{2(1 + 3\ln\frac{R}{\rho}))}{3(2 + \ln\frac{R}{\rho})(1 + \ln\frac{r}{\rho})^2}$

and $\beta_1 = \dfrac{(3 + \ln\frac{R}{\rho})}{2(2 + \ln\frac{R}{\rho})}$; $\beta_2 = \dfrac{2(1 + 2\ln\frac{R}{\rho})}{(2 + \ln\frac{R}{\rho})(1 + \ln\frac{R}{\rho})}$; $\beta_3 = \dfrac{1 + \ln\frac{R}{\rho}}{12(2 + \ln\frac{R}{\rho})}$ (19)

The value of ρ/R is found from (15) or (16) depending on whether a/R is greater or less than $e^{-1/2}$. The coefficients α_1 α_2 β_1 β_2 and β_3 may then be evaluated for various a/R and are given in Table I together with critical values of δ/h. Intermediate values correct to two significant figures may be found by linear interpolation in the range $0.1 \leq a/R \leq 1$. In the neighborhood

Table I: Values of coefficients in the formulas (19) and critical values of δ/h.

a/R	0	0.01	0.1	0.2	0.4	0.6	0.8	1.0
α_1	0	0.323	0.440	0.481	0.519	0.533	0.536	0.535
α_2	0	0.010	0.150	0.196	0.256	0.295	0.317	0.324
β_1	(0.500)	0.591	0.635	0.655	0.681	0.699	0.712	0.716
β_2	(0)	0.646	0.879	0.963	1.038	1.066	1.072	1.071
β_3	(0.0833)	0.0682	0.0609	0.0574	0.0531	0.0501	0.0480	0.0473
δ/h	∞	2.253	1.355	1.109	0.879	0.753	0.681	0.657

Contract DA-19-020-ORD-3172/4
Project TB2-0001 (1086)

of $a/R = 0$, the coefficients α_1 and β_2 fall rapidly to zero and linear interpolation cannot be used. However, the theory is unlikely to be applicable for very small a/R because the effects of shear force are neglected, so in this range the precise values of coefficients are of little interest.

Theory predicts a finite slope for the load-deflection curve immediately after yield. This result is exact in that at zero deflection the velocity field is known to be correct within the framework of the thin plate theory.

Comparison with Tests.

Data is available that enables a comparison to be made between the above theory and the results of static tests of mild steel plates [3]. Fig. (7) shows observed central deflection v, applied load for a series of plates having various ratios of diameter to thickness. Each plate was clamped to a very stiff outer ring and was loaded through a centrally placed punch. Supposing the effects of non-uniformity of pressure beneath the punch to be purely local, the test conditions conform closely to those assumed in the theory. The solid line shows the load-deflection curve computed from (19), using the coefficients for $a/R = 0.1$ given in Table I. For the plates of intermediate thickness, the general character of the post yield behaviour is represented quite well by the theory when due allowance is made for the neglect of elastic deflection. For the thickest plate, the increase in rate of deflection at the yield load is less than expected. This may be due to the approximations of the simple plastic plate theory (e.g. that plane sections remain plane) which are unlikely to be accurate for very thick plates, or to the approximations used for the slope and radii of curvature of the midsurface. For the thinnest plate, the pre-yield and post-yield deflection rates were very similar so no marked change in slope was to be expected at the yield load.

Fig. (8) shows load-deflection data for a plate subject to uniform

pressure. The solid line shows the load-deflection curve computed from (19) using the coefficients for $a/R = 1$, as given in Table I. This case has been studied by means of membrane theory, in which bending action is neglected [15, 16, 17, 18]. The load-deflection relationship obtained in [17] for rigid-ideally plastic material obeying the maximum shear stress criterion of yield has been added to Fig. (8) as the broken line. This is seen to represent the observations quite well over a wide range of deflection, although the theory cannot, of course, give an accurate guide to the rate of deflection in the neighborhood of the yield point load.

Comparison of Figures (7) and (8) suggests that membrane theory might also be of use for very thin plates loaded over only part of the surface. The membrane theory for this slightly more general case is developed in the following section.

4. Theory of Plastic Membranes

Consider a clamped circular plate on which a uniform pressure of intensity p acts over a central area bounded by $r = a$. If bending forces cannot develop, the equations of equilibrium (1) become, for $0 < \varphi < \varphi(a)$,

$$\left.\begin{aligned} \frac{N_\varphi}{r_1} + \frac{N_\theta}{r_2} &= p \cos\varphi \\ N_\varphi &= \frac{1}{r_2 \sin^2\varphi}\, p \int_0^\varphi r_1 r_2 \sin\varphi \, d\varphi \end{aligned}\right\}$$

and for $\varphi(a) < \varphi$,

$$\left.\begin{aligned} \frac{N_\varphi}{r_1} + \frac{N_\theta}{r_2} &= 0 \\ N_\varphi &= \frac{1}{r_2 \sin^2\varphi}\, p \int_0^{\varphi(a)} r_1 r_2 \sin\varphi \, d\varphi \end{aligned}\right\}$$

where $\varphi(a)$ is the value of φ at the radius $r = a$.

When the maximum shear stress criterion of yield is used for the plastically deforming portions of the shell, the stress point with the coordinates N_φ and N_θ will be situated on the yield hexagon shown in Fig. (5). It is easily seen that, when the stress state is represented by one of the sides of the yield hexagon, the unknown stress resultants may be eliminated from the equations of equilibrium to obtain an equation that contains only $r_1(\varphi)$, $r_2(\varphi)$ and p. This last equation is a differential equation which must be satisfied by the meridian curve of the deflected plate. Thus the deflected shape of the plate is very nearly determined by the equations of equilibrium when the type of plastic regime is known. It is to be noted that the corners of the yield hexagon require special treatment, because two equations are obtained for each of the regions of loading that meet at the corner.

Assuming that the slope of the meridian curve remains small, the equations of equilibrium become, for $r < a$

$$\left.\begin{aligned} r\, N_\varphi \frac{d^2 z}{dr^2} + N_\theta \frac{dz}{dr} + pr &= 0 \\ 2\, N_\varphi \frac{dz}{dr} + pr &= 0 \end{aligned}\right\} \tag{20}$$

and, for $a < r < R$

$$\left.\begin{aligned} r\, N_\varphi \frac{d^2 z}{dr^2} + N_\theta \frac{dz}{dr} &= 0 \\ 2r\, N_\varphi \frac{dz}{dr} + pa^2 &= 0 \end{aligned}\right\} \tag{21}$$

At the centre of the plate,

$$N_\theta = N_\varphi = N_0$$

by symmetry. Therefore, for the neighbouring plate elements, the stress state

must be represented by either the regime AB or AF; i.e. $N_\varphi = N_0$, $N_0 \geq N_\theta \geq 0$ or $N_\theta = N_0$, $N_0 \geq N_\varphi \geq 0$. If the first condition is introduced in the equations of equilibrium (21), the second condition gives, for $0 < r \leq a$

$$z = -\frac{pr^2}{4N_0} + \delta \tag{22}$$

where δ is the deflection at the centre. Using these results in the first of (21),

$$N_\theta = N_0 .$$

Similarly, for $r > a$

$$N_\varphi = N_\theta = N_0$$

and

$$z = -\frac{pa^2}{2N_0} \ln \frac{r}{R} \tag{23}$$

where the boundary condition $z = 0$ at $r = R$ is satisfied automatically. The curves defined by (22) and (23) will match at $r = a$ if

$$-\frac{pa^2}{2N_0} \ln \frac{a}{R} = -\frac{pa^2}{4N_0} + \delta$$

Writing the total load as $P = \pi a^2 p$, the load-deflection relationship becomes

$$P = 2\pi N_0 \frac{\delta}{\frac{1}{2} + \ln \frac{R}{a}} . \tag{24}$$

This may be plotted non-dimensionally after dividing through by the yield point load P_L defined in Section 3. The relationship is shown in Fig. (7) as the broken line. This line is in quite good agreement with the data for the thinnest plate, thus illustrating that a membrane type theory may also be of use in certain cases of non-uniform loading.

Contract DA-19-020-ORD-3172/4
Project TB2-0001 (1086)

Concluding Remarks.

To place the results in perspective in relation to limit design [5, 6] it should be noted that the approximate stiff plate theory developed here does not necessarily give an upper bound to the load carrying capacity at a specified central deflection because, in general, the assumed shape of the plate is not exactly correct. We have found upper bounds to a slightly different problem. This point is well illustrated by the case where $a/R = 0.1$, shown in Fig. (7), for which at large deflection the carrying capacity of the membrane exceeds that computed for the stiff plate, presumably because the membrane assumes a more favorable shape. A theorem may exist to the effect that, under certain restrictions, the structure will assume the most favorable shape; but this has not yet been established. In the meantime the best procedure is to judge the utility of the results obtained in specific cases by direct comparison with tests.

The comparisons made with the results of tests on mild steel plates suggest that, for mild steel, there is a substantial range of thicknesses in which the present stiff plate theory represents the immediate post yield behaviour with fair accuracy, when due allowance is made for the neglect of elasticity. For both very thick and very thin plates, however, the results are less satisfactory. This is not unexpected. For very thick plates the assumptions of the simple bending theory of plates will not be met even approximately, whilst for very thin plates, the relatively high rate of elastic deflection tends to mask the change in deflection rate at yield as predicted by the rigid-plastic model. Settlement of the precise range of utility of the rigid-plastic theory must await further tests; however, on the evidence available, it seems likely that the thin plate limit is reached when the elastic slope is about twice the ultimate post-yield slope β_2 (see Table I). When the elastic slope is smaller

than this, a membrane theory is probably better.

The point of greatest general interest emerging from the analysis is that it seems likely the continued strengthening of plates immediately above the yield point load can be largely explained by taking into account the changes in geometry and without postulating strain hardening or other change in the properties of the material as yield proceeds.

Contract DA-19-020-ORD-3172/4
Project TB2-0001 (1086)

REFERENCES

[1] R. M. Haythornthwaite, "The Deflection of Plates in the Elastic-Plastic Range," Brown University Technical Report, OOR-3172/1, to be published in the Proceedings of the Second U. S. National Congress of Applied Mechanics (1954).

[2] R. M. Cooper and G. A. Shifrin, "An Experiment on Circular Plates in the Plastic Range," to be published in the Proceedings of the Second U. S. National Congress of Applied Mechanics (1954).

[3] J. Foulkes and E. T. Onat, Report of static tests of circular mild steel plates: to appear as a Technical Note of the Division of Engineering, Brown University.

[4] R. M. Haythornthwaite, Report of static tests of circular mild steel plates under reversed loading: to appear as a Technical Note of the Division of Engineering, Brown University.

[5] H. J. Greenberg and W. Prager, "Limit Design of Beams and Frames," Proc. Amer. Soc. Civil Engineers, 77, Separate No. 59 (1951).

[6] D. C. Drucker, W. Prager and H. J. Greenberg, "Extended Limit Design Theorems for Continuous Media," Q. Appl. Math., 9, 381-389 (1952).

[7] H. Maier-Leibnitz, "Versuche mit eingespannten und einfachen Balken von I-Form aus St. 37," Bautechnik, 7, 313 (1929).

[8] F. Stüssi and C. F. Kollbrunner, "Beitrag zum Traglastverfahren," Bautechnik, 13, 264 (1935).

[9] J. F. Baker and J. W. Roderick, "Investigation into the Behaviour of Welded Rigid Frame Structures," Trans. Inst. Welding, 1, 206-226 (1938) and 3, 83-92 (1940).

[10] J. F. Baker and J. W. Roderick, "Tests on Full-Scale Portal Frames," Proc. Instn. Civil Engineers, I (Part 1), 71 (1952).

[11] R. Hill, "On the State of Stress in a Plastic-Rigid Body at the Yield Point," Phil. Mag., (7) 42, 868-875 (1951).

[12] R. M. Haythornthwaite and E. T. Onat, "The Load Carrying Capacity of Initially Flat Circular Steel Plates under Reversed Loading," Brown University Technical Report, OOR-3172/5, to be published in Jour. Aeronautical Sciences.

[13] E. T. Onat and W. Prager, "Limit Analysis of Shells of Revolution," Brown University Technical Report DA-798/13 (1954), to be published by the Dutch Academy of Sciences.

[14] H. G. Hopkins and W. Prager, "The Load Carrying Capacities of Circular Plates," J. Mechanics & Physics of Solids, 2 1-13 (1953).

Contract DA-19-020-ORD-3172/4
Project TB2-0001 (1086)

[15] A. N. Gleyzal, "Plastic Deformation of a Circular Diaphragm," Trans. Am. Soc. Mechanical Engineers, 70, 288 (1948).

[16] R. Hill, "A Theory of the Plastic Bulging of a Metal Diaphragm by Lateral Pressure," Phil. Mag., (7) 41, 1133-1142 (1950).

[17] E. W. Ross and W. Prager, "On the Theory of the Bulge Test," Quart. Applied Math., 12 86-91 (1954).

[18] A. S. Grigor'ev, "Investigation of the Work of a Circular Membrane Deformed well Beyond the Elastic Limit," Akad. Nauk S.S.S.R. Inzenernyi Sbornik 9 99-112 (1951) (Russian).

Contract DA-19-020-ORD-3172/4
Project TB2-0001 (1086)

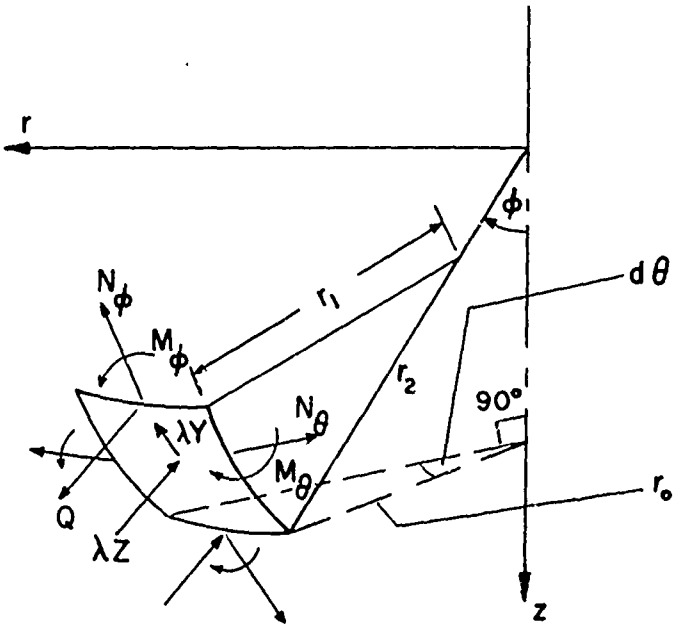
r
ϕ_1
$d\theta$
N_ϕ
r_1
M_ϕ
r_2
N_θ
90°
λY
M_θ
r_o
Q
λZ
z

FIG. 1

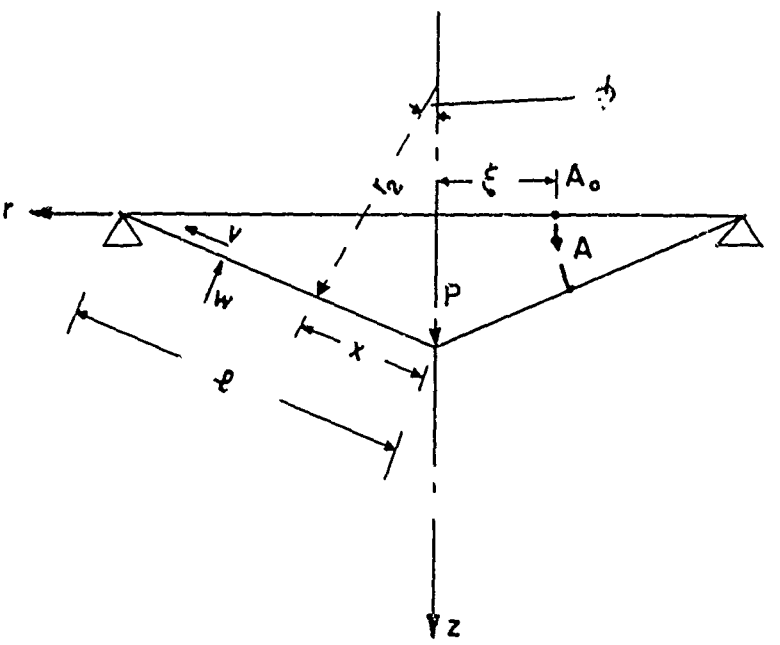
ϑ
r_o
ξ
A_o
r
v
A
w
P
x
ℓ
z

FIG. 2

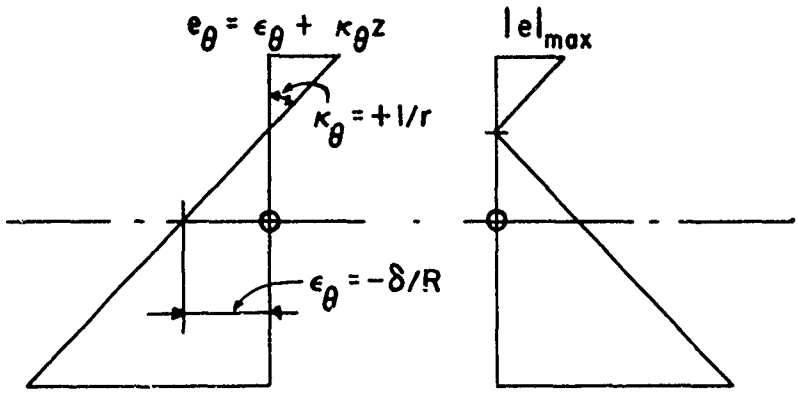

FIG. 3

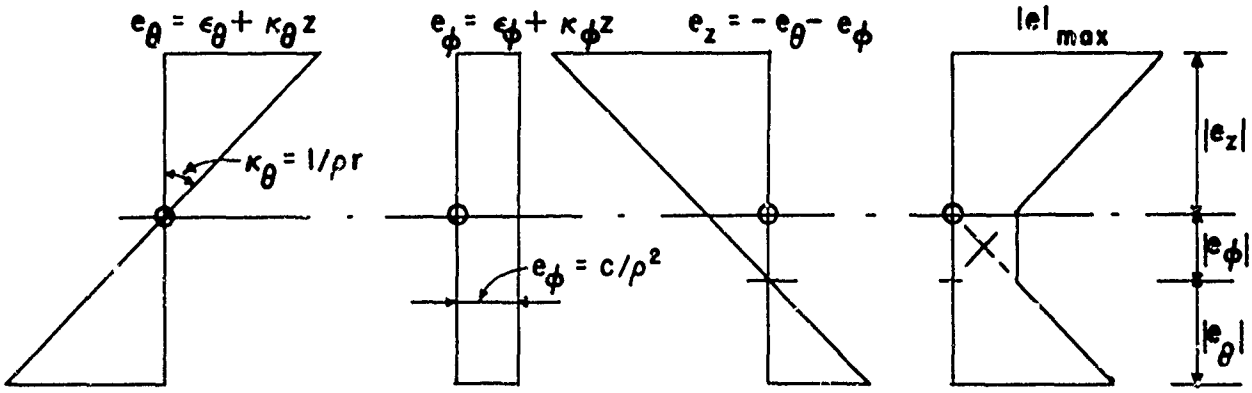

FIG. 4a

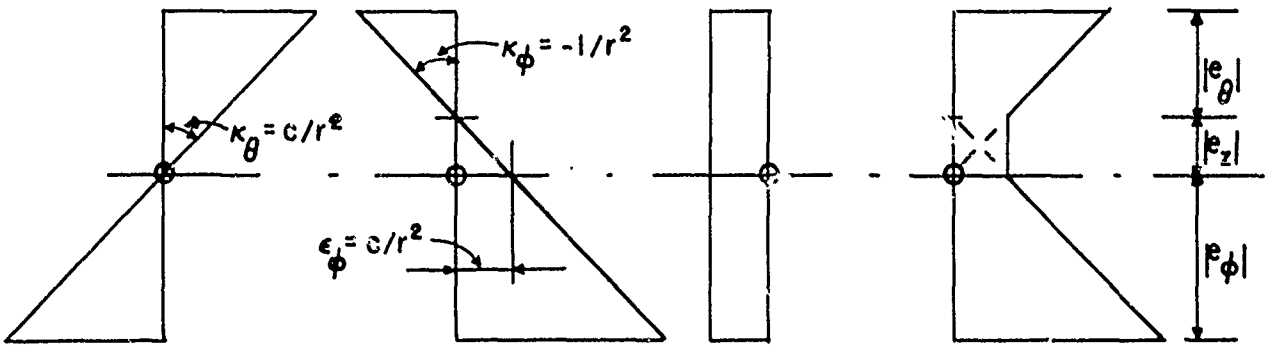

FIG. 4b

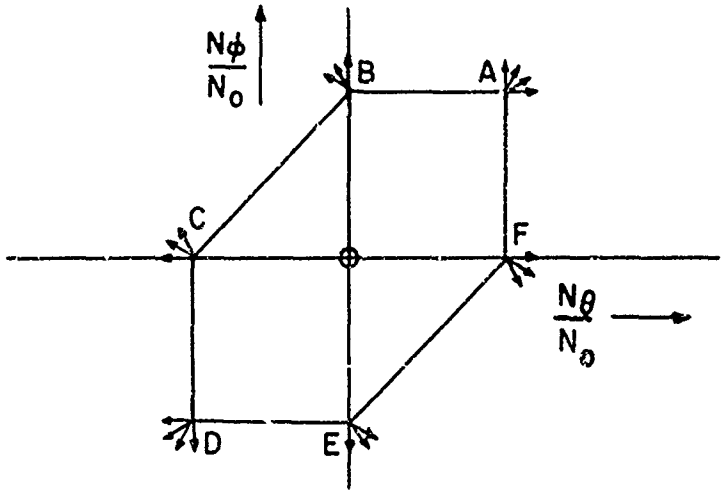

FIG. 5

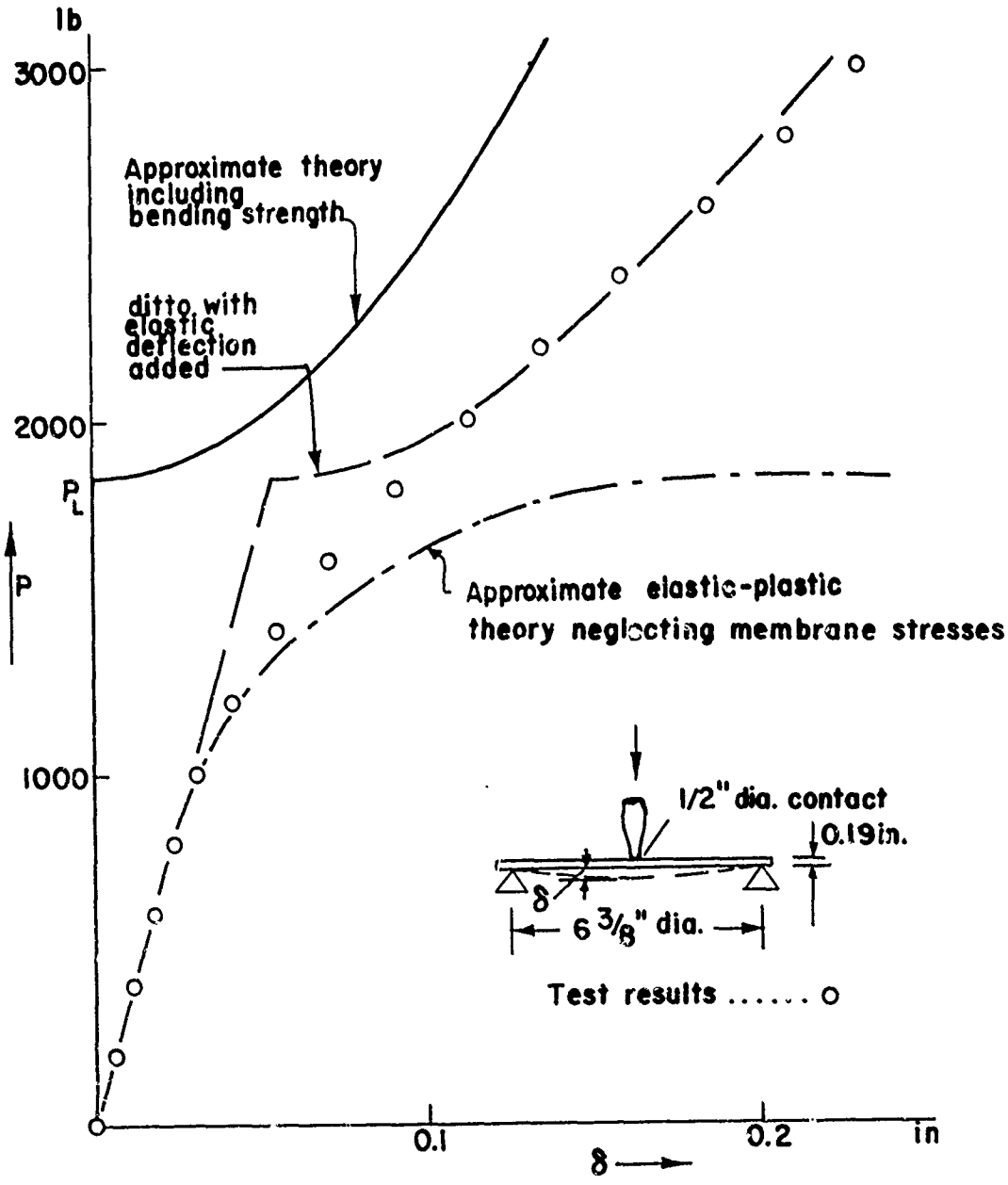

FIG. 6 SIMPLY SUPPORTED MILD STEEL PLATE SUBJECT TO A CENTRAL LOAD

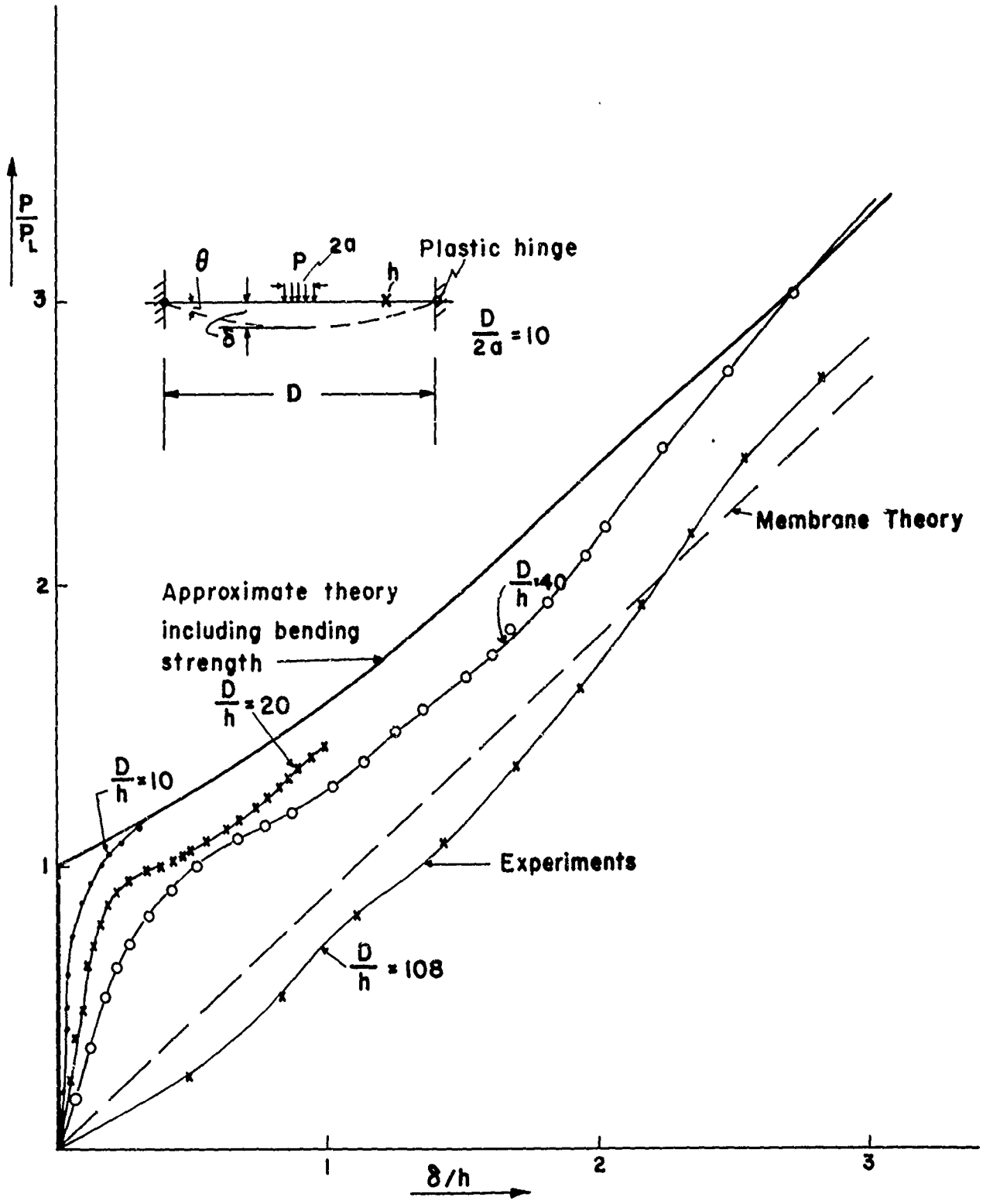

FIG. 7 CLAMPED MILD STEEL PLATES SUBJECT TO A CENTRAL LOAD

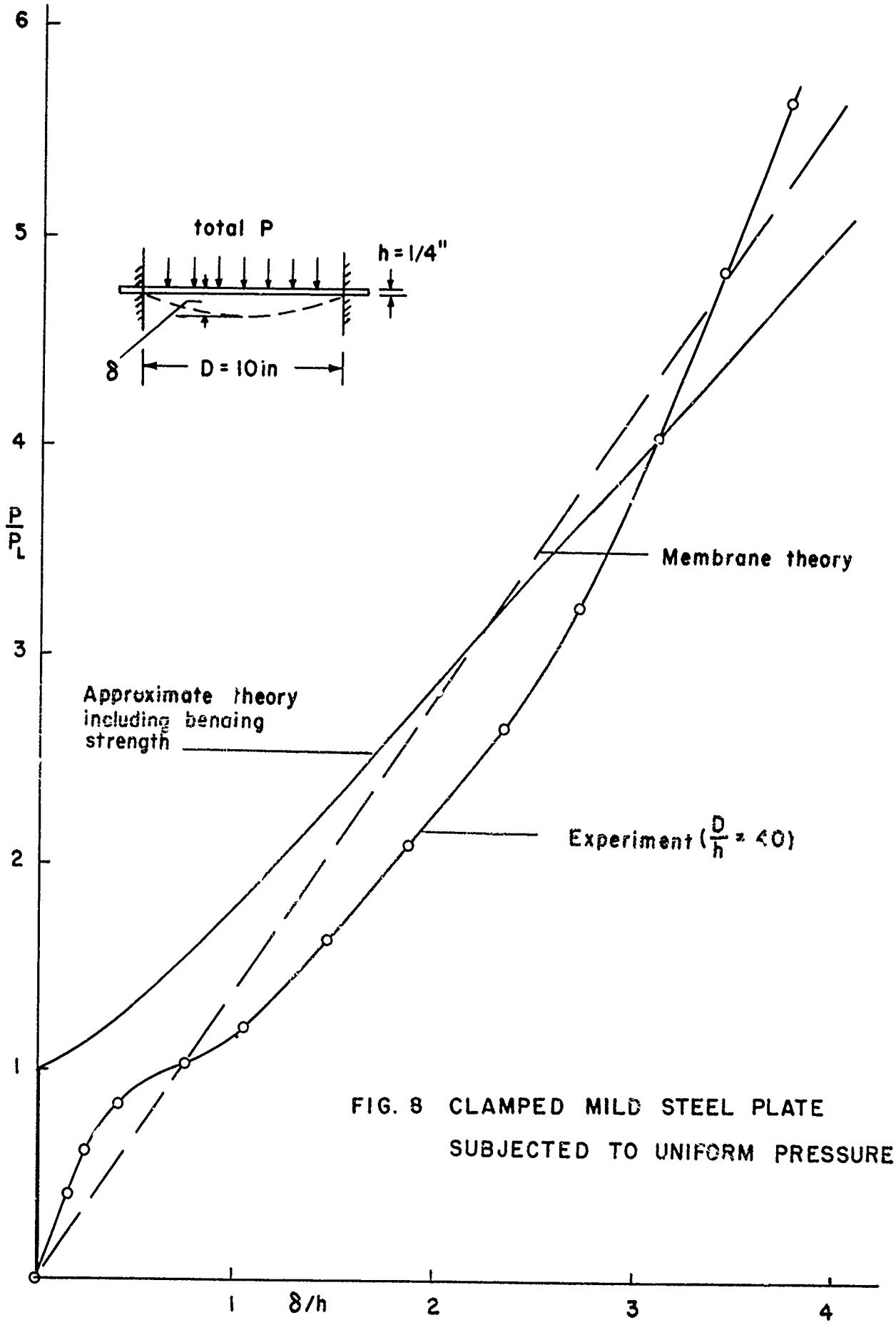

FIG. 8 CLAMPED MILD STEEL PLATE SUBJECTED TO UNIFORM PRESSURE

Contract No. DA-19-020-ORD-3172
Project No. TB2-0001 (1086)

DISTRIBUTION LIST

Number	Agency
2	Chief, Boston Ordnance District Army Base, Boston 10, Mass. Attn: Contracting Officer
1	Director, Applied Physics Lab. John Hopkins University 8621 Georgia Avenue Silver Spring 19, Maryland
1	Commanding General Air University Maxwell Air Force Base, Alabama Attn: Air University Library
1	Canadian Joint Staff 1700 Massachusetts Ave. N.W. Washington 6, D. C. THRU: ORDGU-SE
1	Commanding General Air Res. & Dev. Command P. O. Box 1395 Baltimore 3, Maryland Attn: RDD
1	Commanding General Air Res. & Dev. Command P. O. Box 1395 Baltimore 3, Maryland Attn: RDR
5	Armed Services Tech. Info. Agency Document Service Center Knott Building Dayton 2, Ohio Attn: DSC-SD
1	Commander U. S. Naval Ord. Test Station, Inyokern China Lake, California Attn: Technical Library
1	Commanding General Air Material Command Wright-Patterson Air Force Base Dayton 2, Ohio Attn: F. N. Bubb, Chief Scientist Flight Research Lab.

Number	Agency
4	Commanding Officer Watertown Arsenal Watertown 72, Mass.
1	Technical Reports Library SCEL, Evans Signal Corps Lab. Belmar, New Jersey
1	Commanding Officer Engineer Res. & Dev. Laboratories Fort Belvoir, Virginia
1	Commander U. S. Naval Proving Ground Dahlgren, Virginia
1	Chief, Bureau of Ordnance (AD3) Department of the Navy Washington 25, D. C.
1	U. S. Naval Ordnance Laboratory White Oak, Silver Spring 19, Md. Attn: Library Division
1	Director National Bureau of Standards Washington 25, D. C.
1	Corona Laboratories National Bureau of Standards Corona, California
2	Commanding Officer Frankford Arsenal Bridesburg Station Philadelphia 37, Penna.
1	Technical Information Service P. O. Box 62 Oak Ridge, Tennessee Attn: Reference Branch
1	Commanding Officer Signal Corps Engineering Lab. Fort Monmouth, New Jersey Attn: Director of Research
1	The Director Naval Research Laboratory Washington 25, D. C. Attn: Code 2021
1	Jet Propulsion Laboratory California Institute of Technology 4800 Oak Grove Drive Pasadena 3, California

OOR-3172 - Distribution List, cont'd.

Number	Agency
1	Office of the Chief Signal Officer Engineering & Technical Division Engineering Control Branch Room 2B273, Pentagon Bldg. Washington 25, D. C. Attn: SIGGD
1	NAC for Aeronautics 1724 F Street, N.W. Washington 25, D. C. Attn: Mr. E. B. Jackson, Chief Office of Aeronautical Intelligence
1	Scientific Information Section Research Branch Research & Development Division Office, Assistant Chief of Staff, G-4 Department of the Army Washington 25, D. C.
10	Office of Ordnance Research Box CM, Duke Station Durham, North Carolina
2	Office, Chief of Ordnance Washington 25, D. C. Attn: ORDTB-PS
1	Commanding General White Sands Proving Ground Las Cruces, New Mexico
1	Office of Naval Research Washington 25, D. C. Attn: Engineering
1	Commanding General Aberdeen Proving Ground, Maryland Attn: Technical Information Div.
1	Commanding General Redstone Arsenal Huntsville, Alabama
1	Commanding Officer Rock Island Arsenal Rock Island, Illinois
1	Chief, Ordnance Development Division National Bureau of Standards Washington 25, D. C.

Contract No. DA-19-020-ORD-3172

Project No. TB2-0001 (1086)

DISTRIBUTION LIST

Number	Agency
5	Commanding Officer Office of Ordnance Research Box CM, Duke Station Durham, North Carolina
2	Chief of Ordnance Department of the Army Washington 25, D. C. Attn: ORDTB-PS
1	Commanding General White Sands Proving Ground Las Cruces, New Mexico
1	Office of Naval Research Washington 25, D. C. Attn: Engineering
1	Commanding General Aberdeen Proving Ground Aberdeen, Maryland Attn: Tech.-Information Div.
1	Commanding Officer Rock Island Arsenal Rock Island, Illinois
4	Commanding Officer Watertown Arsenal Watertown 72, Mass.
1	Technical Reports Library SCEL, Evans Signal Corps Lab. Belmar, New Jersey
1	Commanding Officer Engineering Res. & Dev. Laboratories Fort Belvoir, Virginia
1	Commander U. S. Naval Proving Ground Dahlgren, Virginia
1	Chief, Bureau of Ordnance (AD3) Department of the Navy Washington 25, D. C.

Number	Agency
1	U. S. Naval Ordnance Laboratory White Oak Silver Spring 19, Maryland Attn: Library Division
1	Director National Bureau of Standards Washington 25, D. C.
1	Corona Laboratories National Bureau of Standards Corona, California
2	Commanding Officer Frankford Arsenal Bridesburg Station Philadelphia 37, Pennsylvania
1	Technical Information Service P. O. Box 62 Oak Ridge, Tennessee Attn: Reference Branch
1	Commanding General Redstone Arsenal Huntsville, Alabama
1	Commanding Officer Signal Corps Engineering Lab. Fort Monmouth, New Jersey Attn: Director of Research
1	The Director Naval Research Laboratory Washington 25, D. C. Attn: Code 2021
1	Jet Propulsion Laboratory California Institute of Technology 4800 Oak Grove Drive Pasadena 3, California
1	Commanding General Air University Maxwell Air Force Base Alabama Attn: Air University Library
1	Deputy District Chief Boston Ordnance District Army Base, Boston, Mass. Attn: Research & Development Branch

Number	Agency
1	Commanding General Air Res. & Dev. Command P. O. Box 1395 Baltimore 3, Maryland Attn: RDR
1	Commanding General Air Res. & Dev. Command P. O. Box 1395 Baltimore 3, Maryland Attn: RDD
5	Armed Services Tech. Info. Agency Document Service Center Knott Building 4th and Main Streets Dayton 2, Ohio
1	Commanding General Wright-Air Development Center Wright-Patterson Air Force Base Dayton 2, Ohio Attn: F. N. Bubb, Chief Scientist Flight Research Lab.
1	Chief of Ordnance Department of the Army Washington 25, D. C. Attn: ORDGU-SE For Transmittal to: Canadian Joint Staff 2001 Connecticut Avenue, N.W. Washington 25, D. C. Thru ORDGU-SE
1	Office of the Chief Signal Officer Engineering & Technical Division Engineering Control Branch Room 2B273, Pentagon Bldg. Washington 25, D. C. Attn: SIGGD
1	Scientific Information Section Research Branch Research & Development Division Office, Asst. Chief of Staff, G-4 Department of the Army Washington 25, D. C.

Number	Agency
1	NAC for Aeronautics 1724 F Street, N. W. Washington 25, D. C. Attn: Mr. E. B. Jackson Chief, Office of Aeronautical Intelligence
1	Director, Applied Physics Lab. Johns Hopkins University 8621 Georgia Avenue Silver Spring 19, Maryland Attn: Dr. R. C. Herman
1	Office of Naval Research Washington 25, D. C. Attn: Mechanics Branch
1	Commanding Officer and Director David Taylor Model Basin Washington 7, D. C.